Pure Appl. Geophys.

DOI 10.1007/s00024-014-0801-3

Pure and Applied Geophysics

Evolution of Wear and Friction Along Experimental Faults

Y. Boneh,[1,3] J. C. Chang,[1] D. A. Lockner,[2] and Z. Reches[1]

Abstract—We investigate the evolution of wear and friction along experimental faults composed of solid rock blocks. This evolution is analyzed through shear experiments along five rock types, and the experiments were conducted in a rotary apparatus at slip velocities of 0.002–0.97 m/s, slip distances from a few millimeters to tens of meters, and normal stress of 0.25–6.9 MPa. The wear and friction measurements and fault surface observations revealed three evolution phases: A) An initial stage (slip distances <50 mm) of wear by failure of isolated asperities associated with roughening of the fault surface; B) a running-in stage of slip distances of 1–3 m with intense wear-rate, failure of many asperities, and simultaneous reduction of the friction coefficient and wear-rate; and C) a steady-state stage that initiates when the fault surface is covered by a gouge layer, and during which both wear-rate and friction coefficient maintain quasi-constant, low levels. While these evolution stages are clearly recognizable for experimental faults made from bare rock blocks, our analysis suggests that natural faults "bypass" the first two stages and slip at gouge-controlled steady-state conditions.

1. Introduction

Rock faulting is a complex process that occurs by brittle fracturing, coalescence and sliding of multiple fractures, and crushing of fracture-bounded wedges (e.g., Peng and Johnson 1972; Hallbauer *et al.* 1973; Hadley 1975; Tapponnier and Brace 1976; Aydin 1978; Sammis *et al.* 1987; Reches and Lockner 1994; Katz and Reches 2004). Naturally, fault surfaces that form by these processes are irregular, fragmented and rough (Lockner *et al.* 1992; Heesakkers *et al.* 2011a). Field, experimental, and theoretical studies suggest that such irregular and rough surfaces of immature faults evolve into smoother, mature surfaces by a combination of rock wear, shear localization, and flow (Ben-Zion and Sammis 2003; Sagy *et al.* 2007). On the other hand, fault roughness may increase by dynamic branching (Sagy *et al.* 2001) or by linking of fault segments (Candela *et al.* 2011). In the present work, we focus on the transient wear during initial slip along experimental faults.

Wear is the process of material removal from sliding surfaces by mechanical actions (Rabinowicz 1965). Early investigators of wear processes focused primarily on wear of machinery components made of metals (Bowden and Tabor 1939). Nevertheless, it was found later that the basic concepts of metals wear could be applied to brittle rocks wear because asperities interaction was considered the controlling process for both metals and rocks (Wang and Scholz 1994). Archard (1953) suggested that wear between sliding blocks occurs at touching asperities that comprise the real contact area, which is a small fraction of the nominal sliding area (Bowden and Tabor 1939; Dieterich and Kilgore 1994). The asperity-controlled model is a two-body configuration in which the wear is dominated by adhesion, abrasion, and plowing at the touching asperities (Wang and Scholz 1995). Two stages of wear intensity were experimentally recognized: an early stage with transient, high wear-rate that is followed by a steady-state stage with quasi-stable, lower wear-rate (Queener *et al.* 1965; Levy and Jee 1988; Power *et al.* 1988; Wang and Scholz 1994). The early slip, called "running-in", was well-described by Queener *et al.* 1965: "If two new machine parts are subjected to sliding…the wear process…is usually characterized by a high initial wear-rate which gradually diminishes to some steady-state value. …the wear occurring before steady-state…from this 'running-in' process frequently

[1] School of Geology and Geophysics, University of Oklahoma, 100 E Boyd St., Norman, OK 73019, USA. E-mail: reches@ou.edu

[2] US Geological Survey, 345 Middlefield Rd., Menlo Park, CA 94025, USA.

[3] Earth and Planetary Sciences, Washington University, One Brooking Drive, St. Louis, MO 63130, USA.

Published online: 19 April 2014

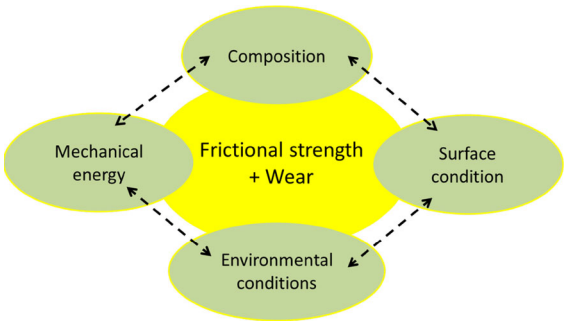

Figure 1
Schematic illustration of conditions and processes that control the frictional strength and fault wear, which are interdependent

represents a significant fraction of the total wear." Queener et al. assumed that during running-in, the wear volume is proportional to the volume available for wear, V, which is the volume bound by the sliding blocks roughness. This assumption led to an expression of the wear-rate, dV/dL,

$$dV/dL = -n \times V$$

where L is the slip distance, and n is a constant parameter that incorporates the loading intensity, slip conditions, and material properties. This equation implies that during running-in, the wear volume is

$$V = V_0 \exp(-nL)$$

where V_0 is the initial volume available for wear. Queener *et al.* (1965) and others (Wang and Scholz 1994) showed that the last equation fits well with experimental results of running-in in both the exponential decrease of wear-rate with slip distance and with proportionality to the initial roughness (equivalent of V_0).

Slip along faults is always associated with frictional resistance that is the integrated effect of adhesion between solid blocks, plastic deformation, and fault wear (Fig. 1). Although wear and friction are two inherently connected processes, and may be seen as two properties of the same process (Rabinowicz 1965; Lyakhovsky *et al*. 2014), their relations are non-unique (Dobson and Wilman 1963; Rabinowicz 1965). Friction strength and wear are related through asperities failure (Wang and Scholz 1994), pulverization at fault tip (Reches and Dewers 2005), evolution of fault surface roughness (Ohnaka, 1973; Santner *et al.* 2006; Brodsky *et al.* 2011), thermal fracturing (Hirose *et al*. 2012), gouge welding (Nakatani 1998), and rock comminution (Wilson *et al*. 2005; Henderson *et al*. 2010).

We present here an experimental analysis of the transient evolution of wear-rate and correlate it to the frictional strength. Our experimental system (Reches and Lockner 2010) allows for continuous quantification of fault friction and wear-rate. Two types of experiments were run: (1) short slip experiments (3–50 mm) designed to characterize early wear processes, and (2) extended slip experiments (up to tens of meters) designed to characterize the evolution of wear and friction to a steady-state condition.

2. Experimental Setting

2.1. Apparatus and Experimental Procedures

We tested experimental faults in a high-velocity rotary apparatus (Reches and Lockner 2010). The samples comprised two solid cylindrical rock blocks; the rotating, lower block had a planar surface and the stationary, upper block had a raised-ring contact (Fig. 2). We used two ring configurations, one with 2.2 and 5.1 cm as inner and outer diameters, respectively, and the other with 5.4 and 7.6 cm as inner and outer diameters, respectively. The apparatus is capable of unlimited slip distance, normal stress up to 35 MPa, and slip velocity from 0.001 to 2 m/s. We continuously monitored the normal stress, shear stress, slip velocity, distance, and temperature at rates of up to 2,000 samples/s. A critical parameter for the analysis is the fault-normal displacement that was measured by two non-contact, eddy-current sensors ($\sim$1 μm resolution) mounted 180° from each other on the sample grips. Samples were ground flat, roughened with #600 SiC grit, and dried for 24 h at 100 °C. The experimental fault blocks were made of five rock types: Tonalite (commercial name Sierra White granite), Kasota dolomite, Karoo gabbro, Blue quartzite and Tennessee sandstone. In each experiment, the fault was loaded to a predetermined normal stress that was maintained at a constant level by a gas/oil accumulator piston system. The slip velocity and duration were prescribed in a command script.

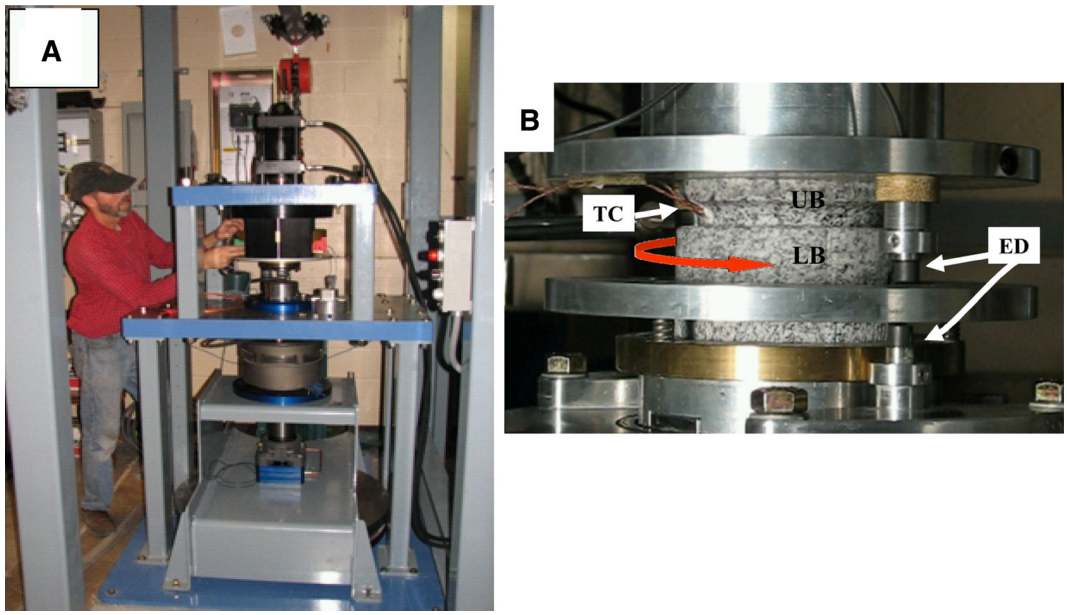

Figure 2
a The rotary shear apparatus, ROGA, of the present study (for details, see text and Reches and Lockner 2010). **b** Sierra White granite sample; UB: upper, stationary block with raised ring shaped bottom that is in contact with LB, the lower, rotating block with planar upper surface; TC: Thermocouples cemented into the upper blocks; ED: Eddy-current sensors that measure the displacements normal to the experimental fault; *red arrow*: rotation sense of the lower block

We present the results of 74 runs at velocities of $V = 0.002$–0.97 m/s, slip distances up to tens of meters, and normal stress of $\sigma_n = 0.25$–6.9 MPa (Table 1). All tests were conducted at room temperature and ambient humidity.

2.2. *Wear Measurements*

Three methods were used to calculate wear: (1) Weight of wear products collected from the sliding surfaces (Wang and Scholz 1994); (2) wear volume determined from fault-normal displacement (Hiratsuka and Muramoto 2005; Hird and Field 2005; Reches and Lockner 2010); and (3) optical measurements of the worn surfaces. We used the second method since it allows continuous measurement of wear without disruption or modification of the fault surfaces.

We continuously measured fault-normal displacement (FND) in an open fault where excess gouge can be ejected out of the slipping surface. The convergence across the fault (FND) is the sum of fault closure/dilation and thermal expansion of the sample blocks due to frictional heating. We removed the thermal effect by the following procedure. For a period of 60–120 s after slip terminated, we monitored sample contraction as FND, and temperature at 3 mm from the sliding surface with embedded one or two thermocouples. Then, for each experiment, we calculated an empirical thermal expansion coefficient (μm/°C) from this post-slip contraction that occurred without sample slip or wear. Finally, this coefficient was used in combination with the measured temperature history during each run to remove the thermal expansion of the sample and yield the net FND due to wear (Reches and Lockner 2010). The accuracy of this linearized, simplified procedure, tested by heating a granite sample with an electric heater (neither slip nor wear) while measuring the temperature and FND in the standard way. The RMS of the difference between calculated and measured thermal FND is 3–10 % of its total.

Wear results are presented in geometric units: Wear is specified by microns of thermally corrected FND, and wear-rate is presented in [μm/m], which is the wear per unit slip. This procedure for wear-rate calculations enables effective analysis of wear evolution for high-velocity and long distances that cannot be done in rock wear studies with short slip distances or very slow slip velocities.

Table 1

General experimental conditions of the present experiments

Experiment no.	Velocity (m/s)	Normal stress (Mpa)	Static friction	Friction (steady-state)	Initial wear-rate	Steady-state wear-rate (μm/m)	Slip distance (m)	Comments
D_1040_1*	0.144, 0.12	1.55	0.87	0.63 ± 0.06	180	53 ± 4	1.9	
D_1040_2*	0.144, 0.12	1.55	0.88	0.65 ± 0.06	75	46 ± 5	1.9	
D_1041	0.144	1.6	0.72	0.53 ± 0.05	55	16 ± 1	14.6	
D_1050_1	0.14	1.85	0.70	0.53 ± 0.04	65	11 ± 3	14.6	
D_1050_2	0.14	1.85	0.72	0.56 ± 0.03	100	28 ± 9	14.6	
D_1012	0.06	1.9	0.82	0.81 ± 0.03	800	201 ± 134	0.6	
D_1370	0.01	0.6	0.87	0.92 ± 0.03	800	205 ± 21	1.1	
D_1450_1	0.015	1.5	0.80	0.83 ± 0.02	3500	961 ± 637	0.1	
D_1504	0.05	0.6	0.93	1.02 ± 0.03	700	12 ± 2	9.0	
D_1510	0.05	0.6	0.98	1.02 ± 0.03	250	12 ± 2	4.5	
D_1280	0.05	3.6	0.75	0.76 ± 0.04	700	104 ± 23	2.3	
G_236	0.07	1.05	0.83	0.41 ± 0.04	105	1.5 ± 0.5	13.0	
G_602	0.046	3.1	0.69	0.42 ± 0.05	95	6.7 ± 1.7	28.1	
G_660	0.045	0.48	0.87	0.43 ± 0.07	1000	2.0 ± 1.0	13.4	
G_661	0.045	0.5	0.98	0.41 ± 0.03	50	1.2 ± 0.8	13.3	
G_670	0.045	2.4	0.81	0.64 ± 0.04	20	1.7 ± 0.8	26.9	
G_720	0.05	2.32	0.67	0.31 ± 0.08	33	1.1 ± 0.9	15.1	
G_760_A	0.03	3.9	0.69	0.33 ± 0.07	16	2.6 ± 8.1	25.0	
G_1551	0.048	1.15	0.70	0.40 ± 0.08	48	4.2 ± 3.2	14.5	
G_1558*	0.004, 0.024	0.94	0.66	0.33 ± 0.08	650	1.0 ± 21	7.7	
G_1561*	0.004, 0.024	2.85	0.69	0.42 ± 0.02	125	12.0 ± 30	8.0	
G_1586*	0.002, 0.03	0.37	0.89	0.46 ± 0.04	17	1.2 ± 2.0	5.5	
G_1587*	0.002, 0.04	0.37	0.93	0.30 ± 0.03	22	6.7 ± 2.4	5.5	
G_1588	0.048	0.43	0.76	0.27 ± 0.01	23	1.0 ± 0.0	28.7	
G_1614*	0.003, 0.042	3.15	0.79	0.40 ± 0.01	160	7.6 ± 4.6	5.5	
G_700	0.05	2	0.71	0.71 ± 0.01	110	4.7 ± 0.6	15.1	
G_740	0.06	3.7	0.70	0.69 ± 0.04	600	42 ± 27	9.6	
G_760	0.05	3.9	0.73	0.70 ± 0.02	650	15.9 ± 0.5	16.4	
D_1010	0.011	2.02	0.75	0.85 ± 0.03	90	92 ± 8	1.3	
D_1013	0.171	1.89	0.8	0.60 ± 0.03	150	114 ± 41	1.1	
D_1030	0.010	1.91	0.86	0.83 ± 0.03	250	299 ± 48	1.1	
D_1250.1	0.010	1.10	0.76	0.88 ± 0.03	−600	52 ± 25	1.1	
D_1250.2	0.010	1.08	0.84	0.84 ± 0.03	250	256 ± 28	1.1	
D_1261	0.032	1.08	0.84	0.90 ± 0.03	5	17 ± 5	3.1	
D_1262	0.063	1.07	0.89	0.90 ± 0.03	20	19 ± 3	3.1	
D_1263.1	0.094	1.06	0.90	0.85 ± 0.03	20	21 ± 3	2.4	
D_1263.2	0.094	1.06	0.91	0.85 ± 0.03	15	26 ± 8	2.4	
D_1265	0.048	1.09	0.91	0.91 ± 0.03	20	17 ± 3	28.0	
D_1270	0.047	3.72	0.72	0.67 ± 0.03	−10	68 ± 16	2.3	
D_1290**	0.047	6.95	0.82	0.62 ± 0.03	200	169 ± 50	1.4	No steady
D_1440	0.048	2.37	0.76	0.67 ± 0.03	250	273 ± 29	1.5	
G_651.5	0.022	2.90	0.68	0.40 ± 0.03		7.4 ± 3.4	22.0	No running
G_662	0.045	0.50	0.75	0.42 ± 0.03		0.6 ± 0.2	13.0	No running
G_663	0.045	0.50	0.94	0.56 ± 0.03		0.5 ± 0.1	12.8	No running
G_664	0.045	0.50	0.96	0.50 ± 0.02		1.1 ± 0.7	13.3	No running
G_700.5	0.05	2.10	0.68	0.34 ± 0.02		0.4 ± 0.3	14.9	No running
G_710	0.05	1.96	0.57	0.39 ± 0.02		2.5 ± 1.7	22.0	No running
G_730	0.05	6.80	0.66	0.72 ± 0.02		2.9 ± 0.7	7.6	No running
G_770	0.04	1.86	0.75	0.35 ± 0.02		8.6 ± 4.7	8.0	No running
G_780.91	0.04	1.50	0.70	0.39 ± 0.02		2.3 ± 1.0	8.2	No running
G_780.92	0.04	1.50	0.38	0.22 ± 0.02		2.3 ± 0.5	8.1	No running
G_1552	0.048	1.15	0.58	0.44 ± 0.02		4.3 ± 1.4	14.4	No running
Q_1430	0.08	2.5	0.67	0.69 ± 0.03			2.7	

Table 1 *continued*

Experiment no.	Velocity (m/s)	Normal stress (Mpa)	Static friction	Friction (steady-state)	Initial wear-rate	Steady-state wear-rate (μm/m)	Slip distance (m)	Comments
Short slip distance experiments								
Ga_1620	0.004	4.9	0.45				0.002	
Ga_1650	0.005	2.2	0.46				0.002	
Q_1630	0.004	3.6	0.63				0.004	
Q_1800	0.004	1.0	0.4				0.003	
Q_1801	0.004	1.0	0.5				0.003	
Q_1802	0.006	1.0	0.53				0.01	
Q_1803	0.003	1.0	0.56				0.011	
Q_1804	0.003	3.1	0.6				0.01	
Q_1805	0.003	3.1	0.64				0.01	
TS_1700	0.003	1.4	0.5				0.0019	
TS_1701	0.003	1.4	0.55				0.007	
Ga_1570	0.002	0.42	0.85				0.057	
Ga_1621	0.004	5.0	0.58				0.0023	
Ga_1622	0.004	5.0	0.57				0.0022	
Ga_1623	0.004	5.0	0.56				0.0022	
Ga_1624	0.004	5.0	0.59				0.008	
Ga_1625	0.004	5.1	0.6				0.112	
Q_1400_1	0.01	0.6	0.73				0.31	
Q_1400_2	0.01	0.6	0.74				0.31	
Q_1630	0.006	3.6	0.63				0.0035	
Q_1631	0.007	3.6	0.64				0.0041	
Q_1632	0.007	3.7	0.62				0.0038	
Q_1720	0.003	2.5	0.59				0.0037	

'No running' comment implies an experiment without running-in stage

G Sierra White Granite, *D* Kasota Dolomite, *Ga* Karoo Gabrro, *Q* Blue Quartzite, *TS* Tennessee sandstone

* indicates an experiment with stepping slip velocity

3. Wear Evolution

The present experiments revealed a contemporaneous evolution of wear and frictional strength. We recognized three stages: An initial stage that was observed only in experiments with small slip distances of $D < 50$ mm, and displayed wear-rates as high as 10^4 μm/m; a running-in stage (Queener *et al.* 1965) that is a long transient stage over slip distances of 0.5–3 m during which both the wear-rate and friction coefficient significantly drop; and a steady-state stage that is characterized by lowest, quasi-constant wear-rate and friction coefficient (Archard 1953).

3.1. Initial Stage: Wear of Individual Asperities

3.1.1 Transition from Original to Effective Roughness

The early wear was studied in 12 runs with small slip distances of $D = 2.2$–47.9 mm, at $\sigma_n = 1$–5 MPa, and slip velocity $V = 0.007$–0.013 m/s (Table 2). Four of these experiments started with bare rock surfaces (fresh after SiC grit roughening), and were opened after the slip for surface inspection and measurement. In eight cases, the initial gouge was removed, and another short distance run was conducted on the same sample without grit roughening. We measured the sample surface roughness, before and after the small slip, with a stylus profilometer Surtronic 3+ (Taylor-Hobson); each measurement included five scan profiles, 12.5 mm long, with typical mean roughness of $R_a = 2.5 \pm 1.2$ μm after the SiC grit roughening (Table 2).

The dominant features in experiments on fresh surfaces are bright, elongated striations (Fig. 3), long, depressed scratch striations, and local, deep pits. The bright striations are composed of powder that is smeared parallel to the slip direction (Fig. 3), and are located next to scratches and pits. For example, the gabbro sample after slip distance of 2.8 mm (Fig. 3a) shows abrasive scratch marks oriented parallel to slip

Table 2

Roughness data of experiments with short slip distance ($D < 50$ mm)

Run no.	Rock type	Normal stress (MPa)	Mean roughness before slip (μm)	Mean roughness after slip (μm)	Before–after mean roughness
1620	Gabbro	5.0	1.76 ± 0.20	3.68 ± 0.99	1.92
1650	Gabbro	2.2	0.68 ± 0.22	1.52 ± 0.87	0.84
1660	Gabbro	1.8	2.08 ± 0.92	1.76 ± 1.08	−0.32
1630	Quartzite	3.6	1.84 ± 0.55	2.72 ± 1.17	0.88
1800	Quartzite	1.0	2.43 ± 0.25	2.11 ± 0.29	−0.32
1801	Quartzite	1.0	2.11 ± 0.29	2.16 ± 0.27	0.05
1802	Quartzite	1.0	2.16 ± 0.27	2.56 ± 0.94	0.41
1803	Quartzite	1.0	2.56 ± 0.94	2.22 ± 0.39	−0.34
1804	Quartzite	3.1	2.22 ± 0.39	2.49 ± 0.25	0.27
1805	Quartzite	3.1	2.49 ± 0.25	2.93 ± 0.55	0.44
1700	Sandstone	1.4	3.92 ± 0.61	3.20 ± 1.06	−0.72
1701	Sandstone	1.4	3.20 ± 1.06	2.69 ± 0.74	−0.51

direction with approximately the same length as the slip distance (2 mm). The measured length of the striations is about equal to the slip distance for small slip experiments, $D = 2$–5 mm, and less than total slip for higher slip experiments, $D > 6$ mm (Fig. 4a). The local, deep damage of these scratches and the spatial association between scratch striations and smeared powder striations (Fig. 3), suggest that these features are the product of plowing by hard grains locked on one side of the fault and act as effective asperities. This highly intensive local wear ends when the asperity grain fails, and the elevated stresses migrate to another large grain or asperity. The deep pits that are associated with the bright powder striation suggest that the powder striations formed by plucking a few grains from the fault surface while leaving the deep pit behind.

The roughness of the original bare surface (maximum summits height of $\sim$0.05 mm, Table 2) is significantly smaller with respect to the localized deep pits and scratch striations (Engelder and Scholz 1976). Thus, the initial stage modifies the surface roughness by particle plucking and smearing (Jackson and Dunn 1974; Moody and Hundley-Goff 1980; Robertson 1982). The comparison between the initial and final fault roughness, R_a, (Table 2) during this stage suggests no roughness change for runs at $\sigma_n < 2$ MPa, and a slight roughening for higher σ_n (Fig. 4b).

3.1.2 Wear Mechanisms

The scratching and roughening during the initial stage (Fig. 4a, b) are associated with distinct stress-dilation events (Fig. 5). The records of fault-normal displacements (FND) of several runs revealed short-lived dilation events during the initial stage (black curves in Fig. 5, and horizontal arrow marked E for one event). These events display temporal dilation magnitudes of 3–15 μm that lasted for slip distances of a few mm to a few cm (Fig. 5 shows only the deviation of FND from its absolute value). The dilation amplitude of the events falls between the mean roughness of $R_a \approx 2.5$ μm, and the height difference between lowest trough and highest peak, 13–54 μm (Table 2). A striking feature of these events is the mimicking relations between the dilation variations and small, transient changes in the normal stress and shear stress; the deviation of the stresses from the global stresses are plotted by blue and red curves, respectively, as function of slip (Fig. 5). The stress deviations are smaller than 0.1 MPa (blue and red vertical scales).

We propose that the simultaneous rise and fall of dilation, shear stress and normal stress reflect slip along a rough fault surface. For simplicity, we consider a local mating contact between two surfaces with similar, sinusoidal rough surfaces (Fig. 6a). As the fault blocks are forced to slip by the applied stresses, the upper block climbs the gentle slope of an asperity (Fig. 6b). This climbing leads to dilation between the blocks (open, black arrows in Fig. 6b), and to a temporal increase of the normal stress.[1] The shear stress also temporarily increases due to the normal stress increase. During the rising phase, the asperity is intact and behaves as a small barrier. Next, the asperity fails and disintegrates (Fig. 6c) leading to temporal drop of the stresses and closure associated with brittle failure. We envision that each dilation event reflects stopping by a set of asperities followed by their failure. To test this mechanism, we plotted

[1] In the present experimental system, a gas-oil actuator that can maintain constant normal stress with variation about 5 % controls the normal stress. Small stress variations, such as in the present events, are not corrected due to seal friction and oil response time.

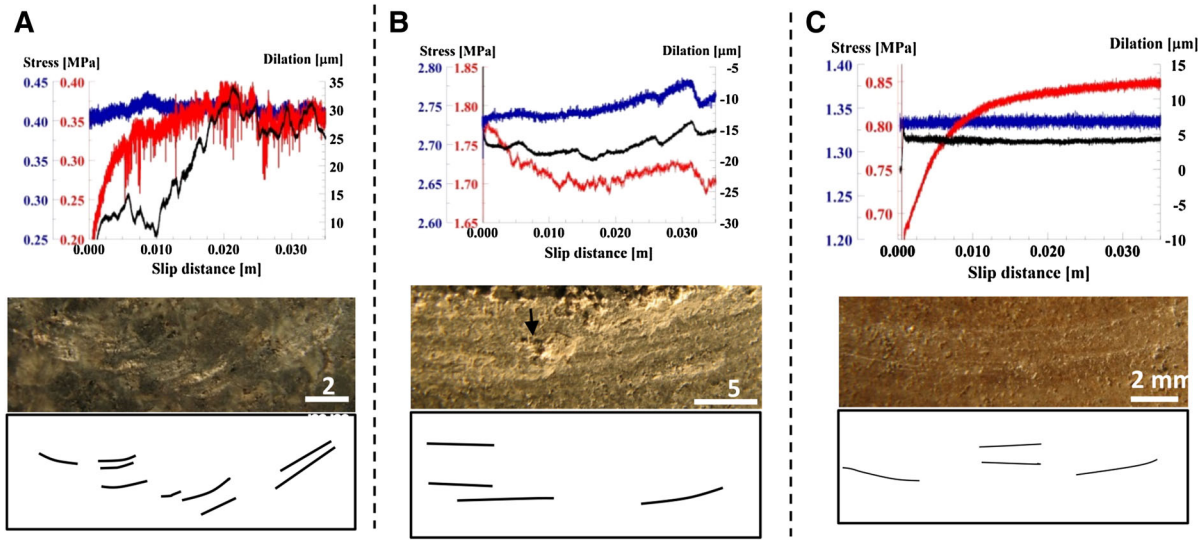

Figure 3

Initial stage observations for the first 35 mm of slip of three sample lithologies: **a** Karoo gabbro, **b** Blue quartzite, **c** and Tennessee sandstone. *Upper panel* displays details of the dilation variations (*black curve*), normal stress (*blue curve*), and shear stress (*red curve*). Note the curves scale as they show the deviations from the global values of the dilation and stresses. Middle panel displays close-up photos of the surfaces of these experimental faults, and the lower panel shows the mapped striations of these fault surfaces. Note that the dilation and stress curves in **a** and **b** are "noisy", whereas the curves are smooth in **c**, and correspondingly, the amount and depth of surface scratches and striations are more pronounced in **a** and **b**; see related discussion in the text on the dilation events during the initial stage

the global shear stress, τ, and normal stress, σ_n, before the events (brown dots, Fig. 4c), and the stress deviations, $\Delta\tau$ and $\Delta\sigma_n$, during the event (local maximum minus local minimum, red dots, Fig. 4c). The slopes on this Mohr diagram, which are the frictional strengths of the rock, indicate $\tau = 0.11 + 0.78 \quad \sigma_n$ before the peak, and $\Delta\tau = 0.03 + 0.67 \ \Delta\sigma$ during the event. Based on the similarity of these strength values, we deduce that similar brittle failure processes control the macroscopic sliding, and the temporary, local failure of asperities.

The above observations suggest that a finite number of touching asperities control the initial wear of a fresh sample. This interpretation is based on the isolated occurrence of the striations and scratches (Fig. 3), and the length similarity of striation and slip distance (Fig. 4a). These asperities were highly loaded (Byerlee 1967a, b; Scholz and Engelder 1976), they failed in a brittle fashion, and their debris was smeared for the total length of the slip distance. This documentation of asperity failure is in agreement with previous studies of wear production through rupture of asperities by plowing, shearing, fracturing and plucking (Bowden and Tabor 1942; Byerlee 1967a, b; Engelder and Scholz 1976; Hundley-Goff and Moody 1980; Moody and Hundley-Goff 1980; Haggert *et al*. 1992; Wang and Scholz 1994; McLaskey and Glaser 2011).

In summary, the distinct features of the initial stage are:

a. During small slip distances (< 50 mm), clear, separate striations develop on a fresh, bare rock surface (Fig. 3).
b. The length of the striations is similar to the total slip, indicating that they form by failure of the larger contacting asperities (Fig. 4a). The striations disappear later, during the running-in stage when many new asperities come into contact and fail.
c. Dilation events with corresponding stress changes (Fig. 5), were recognized only during the initial stage, and they are likely to be associated by deformation and failure of large asperities (Fig. 6).
d. The wear-rates in the initial stage are typically higher by an order of magnitude than wear-rates of the running-in.

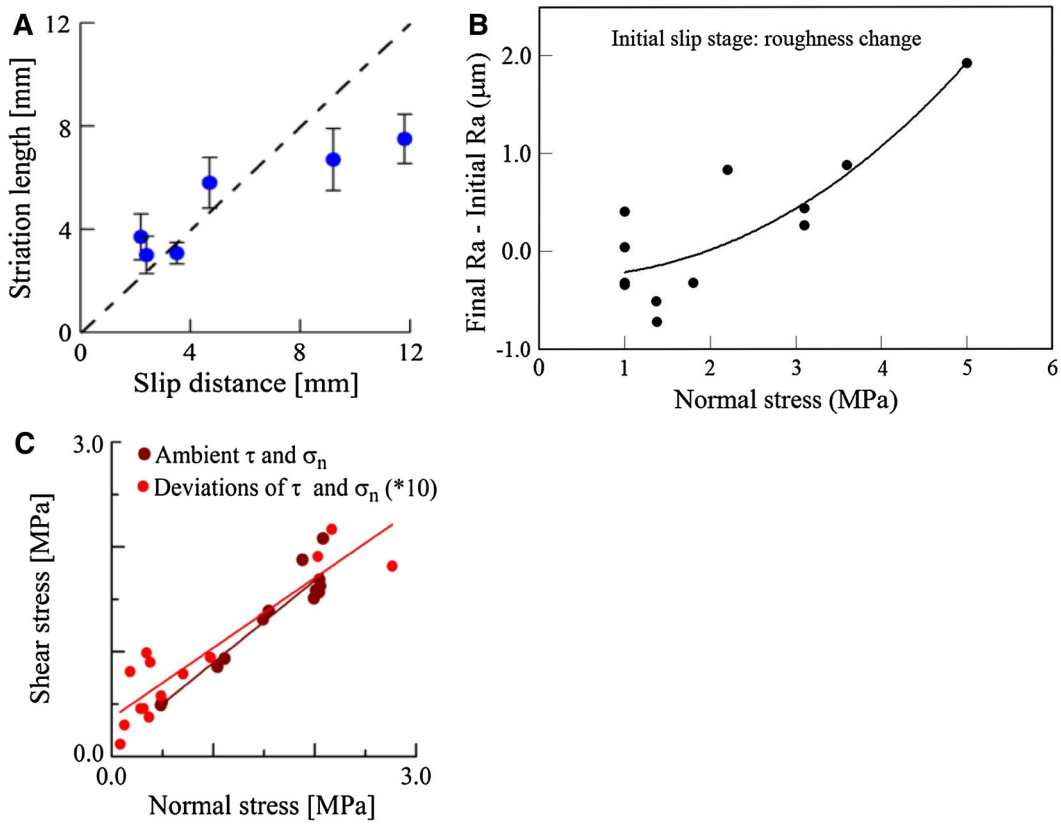

Figure 4

Features of the initial wear stage. **a** Striation lengths as a function of the total slip displacement; each point is the mean value of 10 striations in six separate experiments with standard deviation shown as *error bars*; the *dashed line* represents equality of striation length and slip distance. **b** The change of mean roughness, R_a, during the initial stage as a function of normal stress (Table 2); positive change implies increase of surface roughness. **c** Mohr diagram of the stresses during 13 dilation events (text) in five Kasota dolomite experiments. Global stresses (i.e. the macroscopic stresses during event initiation) are large, *brown dots*, and event stress deviations are small, *red dots*; the corresponding failure envelopes are in *brown* and *red lines*, respectively. The shear and normal stress deviations $\Delta\tau$ and $\Delta\sigma$ are [peak stress—event initial stress]; the smaller stress deviations are multiplied by 10 to allow the same plot for both stress sets. The failure envelopes are similar: $\tau = 0.11 + 0.78\ \sigma_n$, ($R^2 = 0.98$) for the global stresses and $\Delta\tau = 0.03 + 0.67\ \Delta\sigma$ ($R^2 = 0.83$) for the event stress deviations

3.2. Running-in Stage: Wear and Friction Evolution

As mentioned in the Introduction, the running-in stage, as defined by Queener *et al.* (1965), is the stage of intense wear during early sliding along new parts. These authors suggested that the total wear, W, is the sum of the wear contributions of the running-in and the steady-state,

$$W = W_{\text{running-in}} + W_{\text{steady-state}} = A\,[1 - \exp(-nL)] + KL \qquad (1)$$

where A and n and are parameters characteristic for the running-in stage (materials, hardness, normal stress, temperature, and velocity), K is the corresponding parameter for steady-state wear according to Archard (1953), and L is the slip distance. Equation (1) indicates that after a slip distance, L_0, the contribution of the running-in approaches a constant value of $W_0 = A\ [1 - \exp\ (-nL_0)]$, which according to Queener *et al.* (1965) may be a significant fraction of the total wear. This running-in concept fits well with the present results. We analyzed 52 runs of Kasota dolomite and Sierra White granite samples with slip distances >1 m. In 28 runs, the FND indicated closure (= negative dilation) during running-in; eight runs showed dilation during running-in, and 16 runs showed no running-in stage. Out of these experiments, 17 experiments had no pre-existing gouge at the slip surface (either fresh

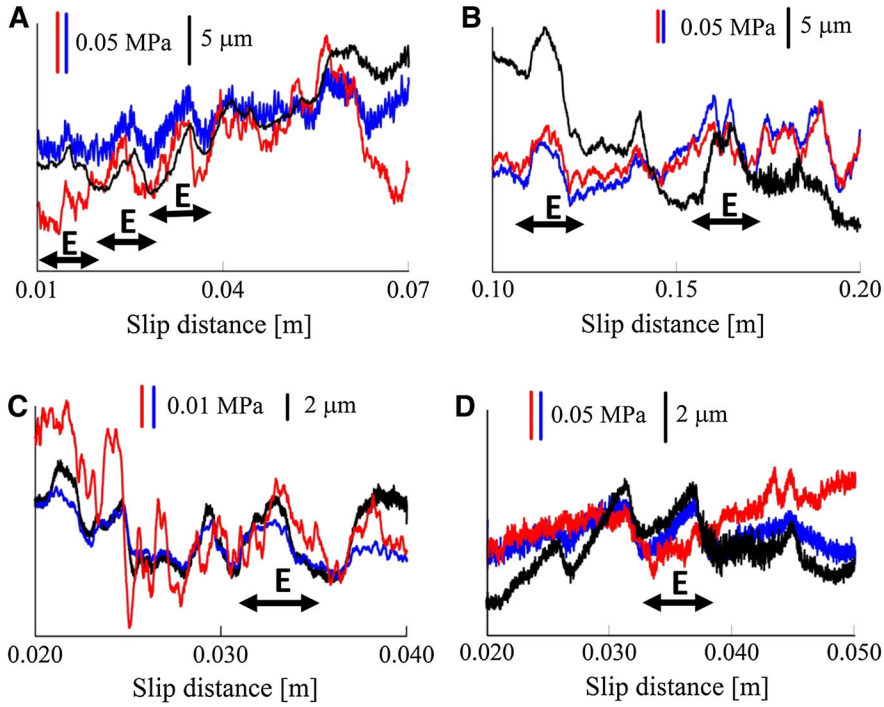

Figure 5

Dilation events during the initial wear stage of four experiments [Kasota dolomite, slip = 10 mm, $\sigma_n = 2.0$ MPa (**a**); Kasota dolomite slip = 100 mm, $\sigma_n = 1.1$ MPa (**b**); Karoo Gabbro, slip = 20 mm, $\sigma_n = 0.4$ MPa (**c**); Blue quartzite, slip = 20 mm, $\sigma_n = 2.7$ MPa (**d**)]. Dilation—*black curves*, shear stress—*red curves*, and normal stress—*blue curves*; *horizontal double-head arrows*, **e** indicates one dilation event. The *curves* are arbitrarily shifted, and show only the deviations from the global values; note the *vertical scale bars* in the corresponding colors

samples or samples in which gouge was removed by air pressure); 13 of the 17 experiments displayed closure running-in and four displayed dilational running-in. In these experiments the total wear fits well with Eq. (1) (Fig. 7) showing a clear transition from running-in to steady-state at $L_0 = 1$–3 m. We consider L_0 the "running-in distance", after which the initial, high wear-rate drops significantly, in agreement with Queener's model. The periodic signal in the wear curves of Fig. 7 (light gray) has a dominant wavelength of $\sim$22 cm, which equals the sample circumference. This signal reflects the sample tilt/wobble, and it is eliminated from the wear calculation by taking a polynomial fit to the dilation curves (Boneh *et al.* 2013).

A striking feature in the present experiments is the parallel evolution of wear and friction during the running-in stage. The curves of total wear, wear-rate and friction coefficient display high values during running-in that systematically and simultaneously decrease to lower, steady-state values. For example, Fig. 8a displays a drop from initial wear-rate of 90 to 5 μm/m over $L_0 \approx 1.8$ m, and the initial friction coefficient, $\mu_i = 1.0$, drops to $\mu_{\text{steady}} = 0.42 \pm 0.05$, over a slip-weakening distance of $d_W \approx 2.75$ m. The range of 1–3 m of the slip-weakening distance in our experiments was commonly observed in rotary shear experiments (Reches and Lockner 2010; Di Toro *et al.* 2011; Brown and Fialko 2012). We determined the L_0 and d_W in all experiments of granite and dolomite with a closure running-in and weakening (20 runs sheared at $\sigma_n = 0.4$–4 MPa and $V = 0.003$–0.14 m/s), and found linear relations between the two parameter (Fig. 8b),

$$L_0 = 0.76 \times d_W, r^2 = 0.70.$$

These observations of wear and friction similar evolution suggest that they are either "cause and effect" or two aspects that depend on the same system conditions (e.g., roughness, mechanical properties, slip

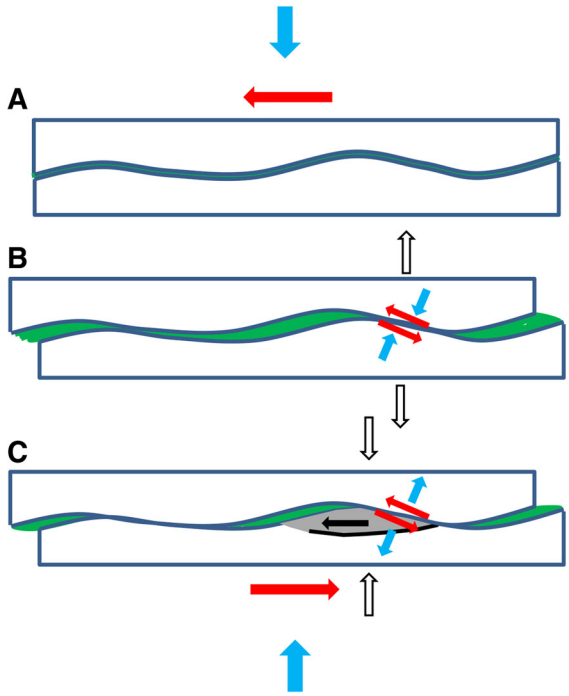

Figure 6
Proposed asperity interaction mechanism for the observed dilation events (Figs. 4c, 5); *green* opening between blocks, *blue arrow* normal stress, *red arrows* shear stress, *open arrows* fault normal displacement. **a** Starting state with locked, mating surfaces. **b** Slip initiates, leading to asperity climbing that causes a temporal dilation and associated stresses increase. **c** Asperity failure (*gray* area with *black arrow*) by shearing off its base leading to temporal closure and stress drops of the event

velocity, and normal stress) (Fig. 1). The analysis of Byerlee (1967a) on granite friction casts light on this wear-friction relation. He showed that the friction of polished surfaces of Westerly granite strongly depends on the roughness: The friction coefficient approached $\mu = 0.2$ for granite surfaces of $R_a = 0.6$ μm, and $\mu = 0.1$, when the granite was sheared against smooth sapphire with $R_a = 0.013$ μm (Fig. 5 in Byerlee 1967a). Byerlee also found that "In contrast to ground surfaces, μ for totally interlocking surfaces of granite…is…$\mu = 1.3$ for $\sigma_n < 6$ MPa, and $\mu = 0.8 + 0.03\sigma_n$ in the range 6 MPa $< \sigma_n <$ 15 MPa" (Byerlee 1967a, Fig. 4). He noted, similarly to our observations, that "In all the experiments the surfaces contained fine white debris after sliding; the amount of debris and the size of the particles increased with the roughness of the surfaces in contact". We propose that the very low friction coefficient of μ = 0.1 of Byerlee (1967a) is the granite frictional strength under negligible wear conditions, and we attribute the much higher friction coefficients ($\mu = 0.8,\ 1.3$) of the interlocking surfaces to energy dissipation by asperity breakage and wear. An upper bound on brittle frictional strength is the internal friction coefficient of 1.4–1.8 (Lockner and Byerlee 1993) determined for an intact rock (= total interlocking) in which the shear is governed by intense micro-fracturing (Reches and Lockner 1994). Similarly, Chen *et al.* (2013) documented friction reduction due to smoothing at the sub-micron scale. This interpretation implies that the weakening during the running-in stage (red curve, Figs. 8a) is primarily due to reduction of wear intensity, in good agreement with the observation of contemporaneous wear and friction evolution. Quantitative relations between frictional work and wear is presented in the "Discussion" below.

3.3. Steady State: The Three-Body Mode

By the end of the running-in stage after slip of L_0, the experimental faults are covered by a continuous gouge layer that fully separates the two rock blocks (Fig. 9a, b). This layer signifies a transition from a two-body frictional mode, which is controlled by asperity wear, to a three-body mode, which is controlled by the gouge frictional strength (Reches and Lockner 2010). This three-body mode is geometrically similar to the well-known *y*-shear surface in fault zones (Gu and Wong 1994). In the present experiments, the steady-state stage is characterized by quasi-constant frictional coefficient with deviations from the mean not exceeding 7 %, and wear-rates with similar variations. The experimental faults have open ring-on-flat configuration, and thus newly worn particles from the sliding surface are free to be ejected. We envision that the gouge layer establishes a quasi-constant thickness during the steady-state stage. In a confined setting, e.g., natural faults, the wear products are trapped and thicken the gouge layer, and consequently may shorten the running-in stage by faster gouge accumulation. Even during steady-state slip, the experimental faults continue to wear by microcracking at the gouge-rock contact (Fig. 9b) in wear-rates that depend on slip velocity, normal stress and lithology (Boneh *et al.* 2013;

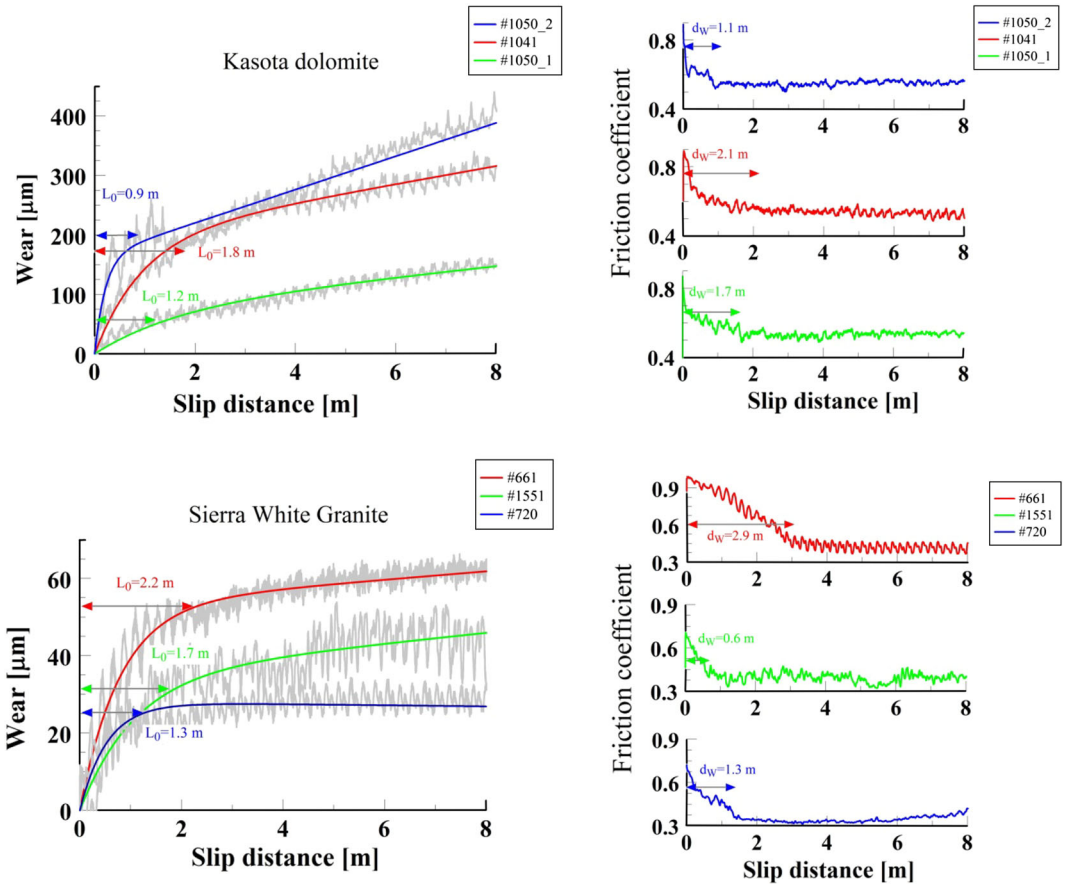

Figure 7

Wear and friction evolution during experiments with Kasota dolomite (*upper plots*), and Sierra White granite (*lower plots*). *Left side* wear-distance evolution (*light gray curves*) with least-square fit of Queener relations (Eq. 1 in text) (*colored*, *smooth curves*), L_0 the slip distance of the transient running-in stage (text). *Right side* the associated friction-distance evolution of the same experiments (corresponding *curves color*), d_W the weakening slip distance (text). The periodic signal (*light gray*) with dominant wavelength of $\sim$ 22 cm reflects the sample tilt/wobble (text). The KD experiments are #1050_2, $\sigma_n = 1.7$ MPa, and $V = 0.14$ m/s; #1041, $\sigma_n = 1.87$ MPa, and $V = 0.14$ m/s; and #1050_1, $\sigma_n = 1.87$ MPa, and $V = 0.14$ m/s. The SWG experiments are #661, $\sigma_n = 0.5$ MPa, and $V = 0.045$ m/s; #1551, $\sigma_n = 1.1$ MPa, and $V = 0.048$ m/s; and #720, $\sigma_n = 2.3$ MPa, and $V = 0.05$ m/s

Lyakhovsky *et al*. 2014). Here, however, we focus on the transient earlier stages of wear-rate and frictional strength.

4. Discussion

4.1. Friction-Wear Relations

The present observations indicate that the reduction of frictional strength strongly correlates with gouge generation and rock comminution. This correlation is manifested by both qualitative similarities (Fig. 7) and quantitative similarities (Fig. 8b), and is supported by the experimental results of Byerlee (1967a). We envision that the work dissipated by asperity failure and rock comminution significantly contributes to the macroscopic frictional strength. Thus, it is our interpretation that the decrease of wear-rate during running-in controls the observed simultaneous fault weakening by reducing energy dissipation. C. Scholz (written communication) suggested that the experimental documentation of the relations between the evolution of frictional

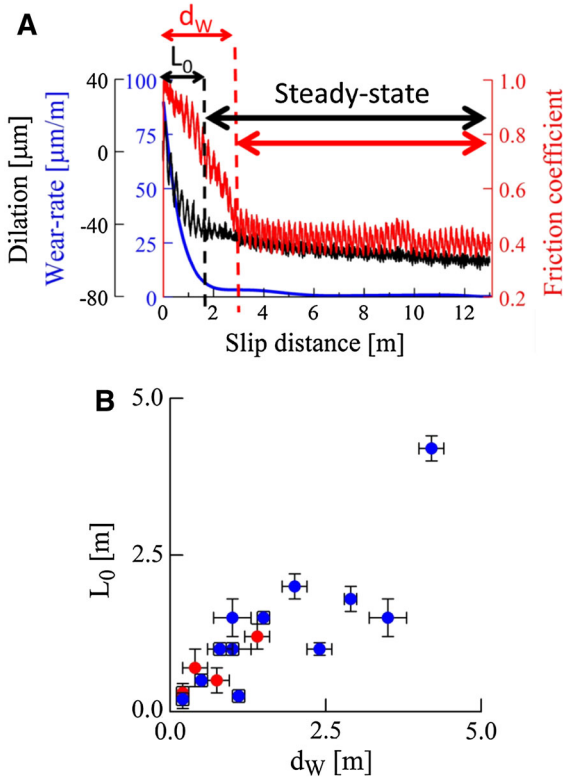

Figure 8
a Friction coefficient (*red*), total wear (*black*) and wear-rate (*blue*) in typical Kasota dolomite experiment, and scales in corresponding colors (text). L_0 the slip distance of the transient running-in stage, d_W the weakening slip distance. **b** L_0 and d_W relations for KD (*red*) and SWG (*blue*) experiments displaying $L_0 = 0.76 \times d_W$ (text)

strength and wear intensity (Figs. 7, 8) allows quantification of the wear contribution to the friction work (also: FULTON and RATHBUN 2011). If the experimental shear work, W_f, is the sum of frictional heat, Q, and gouge surface energy, U_S, then,

$$W_f = \tau u = Q + U_S \quad (2)$$

where τ and u are the shear stress and slip distance, respectively. We assume that at a constant velocity and normal stress, the rate of frictional heating is constant, and it equals the work during steady-state slip, $\tau_1 u$, when the wear-rate is low and may be ignored ($dU_S/du \sim 0$). The surface energy dissipation during the running-in stage can now be calculated from the total wear during this stage. In a typical run of Kasota dolomite in Fig. 7, where $\tau_0 = 1.5$ MPa (initial shear stress), $\tau_1 = 1.0$ MPa (steady-state shear stress), $L_0 = 2$ m (slip distance to reach steady-state of vanishing wear-rate), and $A = 0.002$ m^2 (experimental fault area). We apply the above assumptions to this typical experiment to calculate, the energy dissipation by wear during the experimental running-in:

$$U_s = 0.5\,(\tau_0 - \tau_1)\,AL_0 \times 10^6 = 10^3 J.$$

This dissipation can be compared to the weight of the wear product (gouge). The compaction normal to the fault surface, FND, is a conservative estimate of the total wear, and it is ~50 μm during the running-in of the typical Kasota dolomite experiment (Fig. 7); this compaction corresponds to wear weight of $V_W \sim 0.25$ g. We take a common value for specific surface area of rock minerals, $\gamma = 1$ J/m^2 (KANAMORI and RIVERA 2006), and assume that all the wear energy, U_S, was dissipated by increasing the surface area, S, of the experimental gouge, then,

$$S = (U_S/\gamma)/V_w \sim 4{,}000 \text{ m}^2/\text{g}$$

This value is orders of magnitude larger than surface area measurements of 10–80 m^2/g (WILSON *et al.* 2005). Thus, our conservative assumption of frictional heat and surface area increase (Eq. 2) cannot explain the energetics of the present observations. This result indicates the activity of additional dissipating processes, e.g., disintegration at the crystal structure and amorphization (YUND *et al.* 1990). Studying these processes is beyond the scope of the present analysis.

4.2. Wear Evolution Along Natural Faults

We recognized three evolution stages of the experimental faults. First, an initial stage of small displacements (<50 mm) that is characterized by wear and failure of a few isolated asperities (Figs. 3, 5, 6), and roughening of the fault surfaces (Fig. 4b). Second, a running-in stage of 0.5–3 m slip distance with intense wear (Fig. 7) due to failure at many touching asperities, and simultaneous reduction of the friction coefficient (Figs. 7, 8). Third, a steady-state stage that initiates when the fault surface is covered by a gouge layer (Fig. 9), and the wear-rate and friction coefficient maintain quasi-constant, low levels (Figs. 7, 8). This wear evolution transfers the experimental faults from a two-body shear system to

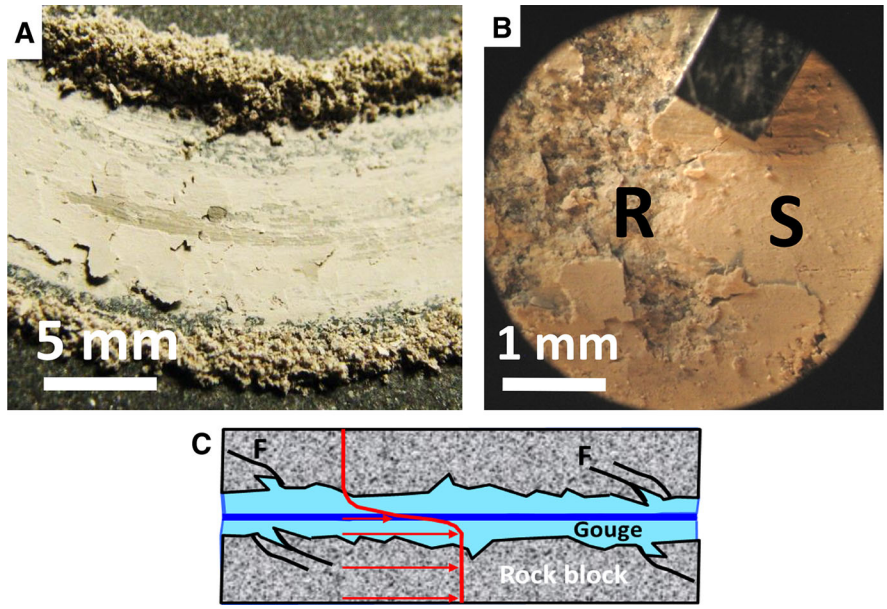

Figure 9
Close-up view of three-body configuration of experimental faults during steady-state slip. **a** Blue quartzite fault, run #1806, after slip of $D = 1.1$ m. Slip surface is covered with smeared, striated gouge with ejected gouge of both side of the slip zone. **b** Close-up view on the sliding surface; *S* a smooth surface of localized slip within the gouge layer that corresponds to the dark blue line in **c**, *R* rough rock surface at a site of gouge removal. **c** Conceptual cross-section of a three-body configuration of a fault. *Gray zones* fractured (F) host rock with rough surfaces (*R* in **b**), *light blue* gouge powder separating the rock blocks, *dark blue* zone of localized slip within the gouge that accommodates most of the slip (*red arrows*) and develops a smooth gouge surface (*S* in **b**)

a three-body system in which the gouge powder separates the two blocks (Fig. 9c). The relevancy of this evolution to faulting of intact rocks and to natural faults is discussed below.

Failure of intact rocks occurs by coalescence of multiple, interacting fractures during fault propagation and the associated crushing of the blocks that bound the fracture zone (Fig. 10a) (Reches and Lockner 1994; Lockner and Byerlee 1993). This process generates a rough fault with a continuous gouge zone made of the crushed blocks and gouge powder (Fig. 10b) (Heesakkers *et al*. 2011b). In this respect, the fault acquires the steady-state geometry (gouge layer in three-body mode) from its onset, in contrast to the 0.5–3 m of slip needed for steady-state along bare, ground rock surfaces. Thus, we anticipate that a new fault in intact rock will display negligible running-in stage, and will slip at quasi-constant friction of the steady-state stage. Servo-controlled triaxial experiments allow exploring the post-failure stage support this prediction. Lockner *et al.* (1992) used the rate of acoustic emission events to prevent catastrophic failure during intact granite faulting. The differential stress in one typical experiment (Fig. 10c) shows about a 30 % drop after peak stress (b–f curve) with an extension of the sample (to prevent catastrophic failure). This drop was associated with sample failure by a through-going fault-zone (Lockner *et al*. 1992). The slip along the new fault occurred at fairly constant differential stress of ~330 MPa. Wawersik and Brace (1971) observed similar behavior (Fig. 10d) when they used a manually operated servo-control to stabilize the post-failure slip. We interpret this behavior as indicating slip under steady-state stage without passing through the earlier running-in stage of bare fault surfaces (Fig. 7).

Natural faults are not composed of bare, planar surfaces, and their wear is not likely to be dominated by ploughing and crushing of asperities. We envision that new natural faults in pristine, intact rock nucleate and grow similarly to experimental faults in intact rock samples (Fig. 10). The gouge zone of such faults develops similarly to intact rock experiments by

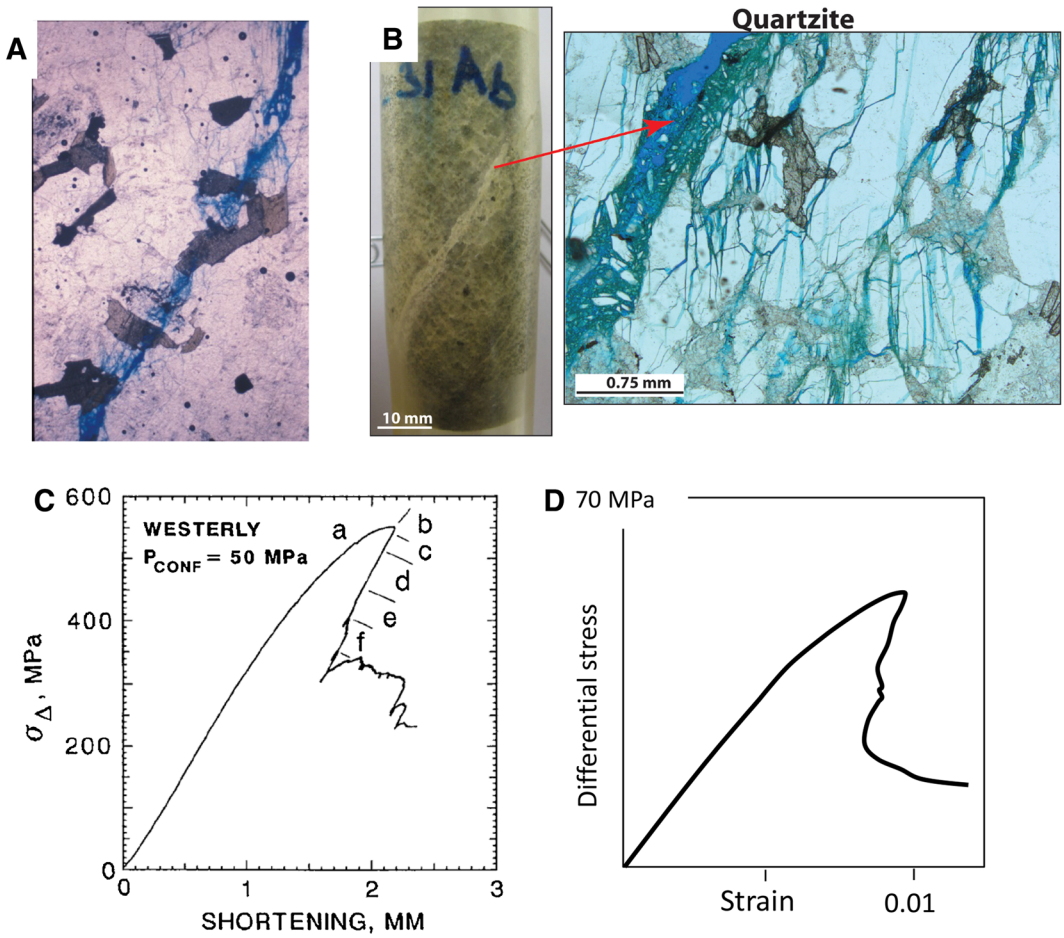

Figure 10

Faulting processes of an intact rock sample. **a** An array of microfractures (*blue* epoxy) at the tip zone of a propagating fault in Westerly granite; thin section view, 2.5 mm wide after Reches and Lockner (1994); $\sigma_n = 50$ MPa, axial shortening in the vertical direction. **b** Experimental fault-zones in quartzite from Pretorius fault, South Africa. Runs under 20 MPa confining pressure. Dilated gouge zone is filled with blue epoxy, and extensive off-fault damage in the quartzite dominated by micro-fractures that branch from the main fault and die away from it; thin-section view after Heesakkers *et al*. (2011b); $\sigma_n = 20$ MPa, axial shortening in the vertical direction. **c** Differential stress during a servo-controlled failure experiment of an intact sample of Westerly granite (Lockner *et al.* 1992). The post-failure sample extension (**b**–**f**) was generated by the servo system to prevent total failure. The post failure slip occurs after point f at fairly constant differential stress. **c** Differential stress during a servo-controlled failure experiment of an intact sample of Westerly granite at confining pressure of 17 MPa [redrawn from Fig. 1 Wawersik and Brace (1971)]

fragmentation and coalescence of multiple micro-cracks in the process zone (Lockner *et al.* 1992; Vermilye and Scholz 1998). For this reason, small faults have relatively thick gouge. For example, Katz *et al.* (2003) mapped small faults in a syenite intrusion, and found that faults with displacements of centimeter scale display gouge zones of millimeter scale (their Fig. 16).

Larger faults wear by more complex processes. The fault-zone undergoes significant healing and cementation between slipping phases, and each slip phase requires the failure of the cemented fault-zone (Tenthorey *et al.* 2003; Muhuri *et al*. 2003; Heesakkers *et al*. 2011a). A new slip phase not only regenerates the three-body structure of the healed gouge-zone, but also wear parts of the adjacent host rocks. The later wear is controlled by two main mechanisms. First, many fault surfaces are fractal (or self-affine) with roughness at all scales (Power *et al.* 1988; Sagy *et al*. 2007). The slip along such irregular

surfaces is expected to continuously wear the protruding asperities (Chester and Chester 2000), leading to a general gouge thickening with increasing fault displacement (Scholz 1987). Second, most faults in the upper crust slip unstably, and unstable rupture propagation leads to intense pulverization and damage in the process zone (Reches and Dewers 2005) as well as in the surrounding crustal rocks (Andrews 2002). This dynamic pulverization may lead to significant widening of the gouge zone (Wilson *et al*. 2003; 2005). For example, a fresh gouge zone of 1–5 mm thickness was formed during earthquake slip of ~25 mm along the Pretorius fault, TauTona Mine, South Africa (Heesakkers *et al*. 2011a), indicating wear-rate of $4–20 \times 10^7$ μm/m. This discussion underscores the complexity of wear along natural faults along which multiple wear mechanisms could operate in during many slip phases.

5. Conclusions

1. Our analysis revealed three evolution stages of the experimental faults:
   a. An initial stage (slip distances <50 mm) of wear by failure of isolated asperities associated with roughening of the fault surface.
   b. A "running-in" stage of slip distances of 1–3 m with intense wear-rate, failure of many asperities, and simultaneous reduction of the friction coefficient and wear-rate.
   c. The steady-state stage initiates when a gouge layer covers the fault surface forming a three-body shear system, and during which both wear-rate and friction coefficient maintain quasi-constant, low levels.
2. The frictional strength and the wear-rate evolves contemporaneously from high initial, high values to lower steady-state levels; this parallel evolution occurs during slip-distances of 1–3 m. We interpret the fault weakening as indicating a reduction of energy dissipation rate by the dropping wear-rate during the running-in stage.
3. The above stages were observed along experimental faults that before shearing were bare rock surfaces, which are nominally planar and relatively smooth (mean roughness of ~2.5 μm). However, spontaneous faults, both in failure experiments of intact rocks and in the field, are much rougher and contain gouge layers from their incipience. We thus envision that the initial and running-in stages may not be realized along natural faults that always slip with as existing gouge layer.

Acknowledgments

We benefitted from help and advice of Andrew Madden and Xiaofeng Chen, University of Oklahoma. We had fruitful discussions with Emily Brodsky, UC Santa Cruz; Chris Scholz, Lamont-Doherty Institute; Amir Sagy, Israel Geological Survey; Einat Aharonov and Shalev Siman-Tov, the Hebrew University. Eric Ferre of Southern Illinois University kindly provided the Karoo gabbro sample. The manuscript was greatly improved by the constructive comments of Chris Scholz and an anonymous reviewer. The study was supported by the NSF, Geosciences, Equipment and Facilities, Grant No. 0732715, and partial support of NSF, Geosciences, Geophysics, Grant No. 1045414, and ConocoPhillips Foundation grant.

References

Andrews, D. J. (2002), *A fault constitutive relation accounting for thermal pressurization of pore fluid*, J. Geoph. Res., *107*, 2363.

Archard, J. F. (1953), *Contact and rubbing of flat surfaces*, J. Appl. Phys., *24*, 981–988.

Aydin, A. (1978), *Small faults formed as deformation bands in sandstone*, Pure Appl. Geophys., *116*, 913–930.

Ben-Zion, Y., and C. Sammis (2003), *Characterization of fault zones*, Pure Appl. Geophys., *160*, 677–715.

Boneh, Y., A. Sagy, and Z. Reches, (2013), *Frictional strength and wear-rate of carbonate faults during high-velocity, steady-state sliding*, Earth Planet. Sci. Lett., V. *381*, P. 127–137.

Bowden, F. P., and D. Tabor (1939), *The area of contact between stationary and between moving surfaces*, Proc. R. Soc. London, *169* (938), 391–413.

Bowden, F. P., and D. Tabor, (1942), *Mechanism of metallic friction*, Nature, *150*, 197–199.

Brown, K. M., and Y, Fialko, (2012), *"Melt welt" mechanism of extreme weakening of gabbro at seismic slip rates,* Nature *488*, 7413, 638–641.

Brodsky, E. E., J. J. Gilchrist, A. Sagy, and C. Collettini, (2011), *Faults smooth gradually as a function of slip*, Earth Planet. Sci. Lett., *302*, 185–193.

Byerlee, J. D. (1967a), *Theory of friction based on brittle fracture*, J. Appl. Phys., *38*, 2928.

Byerlee, J. D. (1967b), *Frictional characteristics of granite under high confining pressure*, J. Geophys. Res., *72*, 3639–3648.

Candela, T., F. Renard, M. Bouchon, J. Schmittbuhl, and E. E. Brodsky (2011), *Stress drop during earthquakes: effect of fault roughness scaling*, Bull. Seismol. Soc. Am., *101*/5, 2369–2387.

Chen, X., Madden, A. S., Bickmore, B. R., and Reches, Z. (2013) *Dynamic weakening by nanoscale smoothing during high.* Geology. V. *41*, p. 739–742.

Chester, F. M., and J. S. Chester (2000), *Stress and deformation along wavy frictional faults*, J. Geophys. Res., *105*, 23,421–423,430.

Di Toro, G., R. Han, T. Hirose, N. De Paola, S. Nielsen, K. Mizoguchi, F. Ferri, M. Cocco, and T. Shimamoto (2011), *Fault lubrication during earthquakes*, Nature, *471*/7339, 494–498.

Dieterich, J. H., and B. D. Kilgore (1994), *Direct observation of frictional contacts: New insights for state-dependent properties,* Pure Appl. Geophys., *143*, 283–302.

Dobson, P. S., and H. Wilman, (1963), *The friction and wear, and their inter-relationship, in abrasion of a single crystal of brittle nature*, Br. J. Appl. Phys., *14*, 132–136.

Engelder, T., and C. H. Scholz (1976), *The role of asperity indentation and ploughing in rock friction- II. Influence of relative hardness and normal load,* Int. J. Rock Mech. Min. Sci. & Geomech., *13*, 155–163.

Fulton, P. M., and A. P. Rathbun (2011), *Experimental constraints on energy partitioning during stick–slip and stable sliding within analog fault gouge*, Earth Planet. Sci. Lett., *308*/1, 185–192.

Gu, Y., and T. F. Wong (1994), *Development of shear localization in simulated quartz gouge: Effect of cumulative slip and gouge particle size*, Pure Appl. Geophys, *143*/1–3, 387–423.

Hadley, K. (1975), *Dilatancy: Further studies in crystalline rocks*, Ph.D. thesis, Mass. Inst. Technol., Cambridge.

Haggert, K., S. J. Cox, and M. W. Jessell (1992), *Observation of fault gouge development in laboratory see-through experiments*, Tectonophysics, *204*/1, 123–136.

Hallbauer, K., H. Wagner, and N. G. W. Cook (1973), *Some observations concerning the microscopic and mechanical behaviour of quartzite specimens in stiff, triaxial compression tests,* Int. J. Rock Mech. Min. Sci., *10*/6, 713–726.

Heesakkers, V., S. Murphy, and Z. Reches (2011a), *Earthquake rupture at focal depth, part I: Structure and rupture of the Pretorius fault TauTona mine South Africa*, Pure Appl. Geophys., *168*/12, 2395–2425.

Heesakkers, V., S. Murphy, D. A. Lockner, and Z. Reches (2011b), *Earthquake rupture at focal depth, Part II: Mechanics of the 2004 M2. 2 Earthquake along the Pretorius Fault, Tautona mine, South Africa*. Pure Appl. Geophys., *168*/12, 2427–2449.

Henderson, I. H., G. V. Ganerød, and A. Braathen (2010), *The relationship between particle characteristics and frictional strength in basal fault breccias: Implications for fault-rock evolution and rockslide susceptibility*. Tectonophysics, *486*/1, 132–149.

Hiratsuka, K. I., and K. I. Muramoto (2005), *Role of wear particles in severe–mild wear transition*, Wear, *259*/1, 467–476.

Hird, J. R., and J. E. Field (2005), *A wear mechanism map for the diamond polishing process*, Wear, *258*/1, 18–25.

Hirose, T., K. Mizoguchi, and T. Shimamoto (2012), *Wear processes in rocks at slow to high slip rates*, J. Struct. Geol., *38*, 102–116.

Hundley-Goff, E. M., and J. B. Moody (1980), *Microscopic characteristics of orthoquartzite from sliding friction experiments. I. Sliding surface*, Tectonophysics, *62*/3, 279–299.

Jackson, R. E., and D. E. Dunn (1974), *Experimental sliding friction and cataclasis of foliated rocks*, Int. J. Rock Mech. Sci. & Geomech. Abstr., *11*/6, 235–249.

Kanamori, H., and L. Rivera, (2006), *Energy partitioning during an earthquake*. Geophys. Mono. Ser., *170*, 3–13.

Katz, O., and Z. Reches (2004), *Microfracturing, damage and failure of brittle granites*. J. Geophy. Res. *109*, doi:10.1029/2002JB001961.

Katz O., Z. Reches, and G. Baer (2003), *Faults and their associated host rock deformation: Structure of small faults in a quartz-syenite body, southern Israel*. J. Structural Geology, *25*, 1675–1689.

Levy, A. V., and N. Jee, (1988), *Unlubricated sliding wear of ceramic materials*, Wear, *121*/3, 363–380.

Lockner D. A., J. D. Byerlee, V. Kuksenko, A. Ponomarev, and A. Sidrin (1992), *Observations of quasi-static fault growthfrom acoustic emissions*, in Fault Mechanics and TransportProperties of Rocks, edited by B. Evans and T.-f. Wong, 3–31.

Lockner, D. A., and J. D. Byerlee (1993), *How geometrical constraints contribute to the weakness of mature faults*, Nature, *363*, 250–252, doi:10.1038/363250a0.

Lyakhovsky, V., A. Sagy, Y. Boneh, and Z. Reches (2014), *Fault wear by damage evolution in a three-body slip mode,* Pure Appl. Geophys, this volume.

McLaskey, G. C., and S. D. Glaser (2011), *Micromechanics of asperity rupture during laboratory stick slip experiments*, Geophy. Res. Lett., *38*/12, doi:10.1029/2011GL047507.

Moody, J. B., and E. M. Hundley-Goff, (1980), *Microscopic characteristics of orthoquartzite from sliding friction experiments. II. Gouge,* Tectonophysics, *62*, 301–319.

Muhuri, S.K., T. A. Dewers, T. E. Scott, and Z. Reches (2003), *Interseismic fault strengthening and earthquake-slip instability: Friction or cohesion?*, Geology, *31*/10, 881–884.

Nakatani, M. (1998), *A new mechanism of slip weakening and strength recovery of friction associated with the mechanical consolidation of gouge*, J. Geophys. Res., *103*/B11, 27239–27256.

Ohnaka, M. (1973), *Experimental studies of stick-slip and their application to the earthquake source mechanism*, J. Phys. Earth, *21*(3), 285–303.

Peng, S., and A. M. Johnson (1972), *Crack growth and faulting in cylindrical specimens of chelmsford granite,* Int. J. Rock Mech. Min. Sci., *9*/1, 37–42.

Power, W. L., T. E. Tullis, and J. D. Weeks (1988), *Roughness and wear during brittle faulting,* J. Geophys. Res., *93*, 15268–15278.

Queener, C. A., T. C. Smith, and W. L. Mitchell (1965), *Transient wear of machine parts,* Wear, *8*, 391–400.

Rabinowicz, E. (1965), *Friction and wear of materials*, John Wiley, New York.

Reches, Z., and D. A. Lockner (1994), *Nucleation and growth of faults in brittle rocks*, J. Geophys. Res. Solid Earth (1978–2012), *99*/B9, 18159–18173.

Reches, Z., and T. A. Dewers, (2005), *Gouge formation by dynamic pulverization during earthquake rupture*, Earth Planet. Sci. Lett., *235*, 361–374.

Reches, Z., and D. A. Lockner (2010), *Fault weakening and earthquake instability by powder lubrication,* Nature, *467*, 452–456.

ROBERTSON, E. C. (1982), *Continuous formation of gouge and breccia during fault displacement*, In The 23rd US Symposium on Rock Mechanics (USRMS).

SAGY, A., Z. RECHES, and I. ROMAN (2001), *Dynamic fracturing: field and experimental observations*, J. Struct. Geol., *23*/8, 1223–1239.

SAGY, A., E. BRODSKY, and G. J. AXEN (2007), *Evolution of fault-surface roughness with slip*, Geology, *35*, 283–286. doi:10.1130/G23235A.1.

SAMMIS, C, G. KING, and R. BIEGEL (1987), *The kinematics of gouge deformation*, Pure Appl. Geophys., *125*, 777–812.

SANTNER, E., D. KLAFFKE, K. MEINE, CH. POLACZYK, and D. SPALTMANN (2006), *Effects of friction on topography and* vice versa, Wear, *261*/1, 101–106.

SCHOLZ, C. H. (1987), *Wear and gouge formation in brittle faulting,* Geology, *15*:, 493–495.

SCHOLZ, C. H., and J. T. ENGELDER, (1976), *The role of asperity indentation and ploughing in rock friction—I: Asperity creep and stick-slip*, Int. J. Rock Mech. Sci. & Geomech. Abstr., *13*/5, 149-154.

TAPPONNIER, P., and B. F. BRACE (1976), *Development of stress induced microcracks in Westerly granite*, Int. J. Rock Mech. Sci. & Geomech. Abstr., *13*, 103–112.

TENTHOREY, E., S. F. COX, and H. F. TODD, (2003), *Evolution of strength recovery and permeability during fluid–rock reaction in experimental fault zones*, Earth Planet. Sci. Lett., *206*/1, 161–172.

VERMILYE, J. M., and C. H. SCHOLZ (1998), *The process zone: A microstructural view of fault growth,* J. Geoph. Res., *103*(B6), 12223–12237.

WANG, W. B., and C. H. SCHOLZ (1994), *Wear Processes During Frictional Sliding of Rock - a Theoretical and Experimental-Study*, J. Geoph. Res., *99*(B4), 6789–6799.

WANG, W.B., and C. H. SCHOLZ (1995), *Micromechanics of rock friction .3. Quantitative modeling*, J. Geoph. Res., *100*, 4243-4247.

WAWERSIK, W. R., and W. F. BRACE (1971), *Post-failure behavior of a granite and diabase*, Rock Mechanics, *3*/2, 61–85.

WILSON, J. E., J. S. CHESTER, and F. M. CHESTER (2003), Micro-fracture analysis of fault growth and wear processes, Punchbowl fault, San Andreas system, California, J. Struct. Geol., *25*, 1855–1873.

WILSON, B., T. DEWERS, Z. RECHES, and J. BRUNE (2005), *Particle size and energetics of gouge from earthquake rupture zones*, Nature, *434*/7034, 749–752.

YUND, R. A., BLANPIED, M. L., TULLIS, T. E. & WEEKS, J. D. *Amorphous material in high strain experimental fault gouges.* J. Geophys. Res. *95*, 15589–15602 (1990).

(Received August 16, 2013, revised January 31, 2014, accepted February 13, 2014)